Research Square

Preprints are preliminary reports that have not undergone peer review.
They should not be considered conclusive, used to inform clinical practice,
or referenced by the media as validated information.

Integrated Experimental and In-Silico Analysis Reveals Melittin as a Modulator of IL-37a-Associated Networks in Neuroblastoma

Berkay ERTAN
Ankara Yıldırım Beyazıt University
Tugba YALCİNKAYA
Ministry of Health
Elif ERCAN
Ankara Yıldırım Beyazıt University
Ahmet CARHAN
acarhan@aybu.edu.tr

Ankara Yıldırım Beyazıt University

Research Article

Keywords: Docking, IL-37a, In silico, Inflammation, Melittin, Neuroblastoma, SH-SY5Y

Posted Date: March 2nd, 2026

DOI: https://doi.org/10.21203/rs.3.rs-8647916/v1

License: This work is licensed under a Creative Commons Attribution 4.0 International License.
Read Full License

Additional Declarations: No competing interests reported.

Version of Record: A version of this preprint was published at The Protein Journal on June 9th, 2026.
See the published version at https://doi.org/10.1007/s10930-026-10341-9.

Abstract

Background: Neuroinflammation is a key process shaping tumor progression and cellular stress responses. Pro-inflammatory signaling components amplify these responses, whereas IL-37a functions as an endogenous suppressor that limits inflammation. Melittin is a bioactive peptide with cytotoxic and immunomodulatory properties; however, its effects on IL-37a-centered immune regulation in neuroblastoma cells remain unclear.

Methods: Human SH-SY5Y neuroblastoma cells were exposed in vitro to melittin at concentrations of 1–32 μM for 24 and 48 h. Cytotoxicity was assessed using the MTT assay. Transcriptional changes in IL-37a-associated signaling components were quantified by qRT-PCR. Pathway-level interactions were analyzed using STRING-based protein–protein interaction networks, Gene Ontology, and KEGG pathway enrichment. The binding potential of melittin to STAT3 and IL-1R8 was evaluated by molecular docking, and in silico ADMET properties were predicted.

Results: Melittin induced dose- and time-dependent cytotoxicity in SH-SY5Y cells, with an IC_{50} of 16 μM at 24 h. Melittin significantly increased IL-37a, IL-18R1, and IL-1R8 expression while suppressing NF-κB, STAT3, MyD88, and Smad3. Caspase-1 expression was elevated, indicating modulation of inflammation-associated cell death pathways. Extracellular matrix remodeling was differentially regulated, with upregulation of MMP-2 and downregulation of MMP-9. Multivariate analyses revealed a treatment-specific transcriptional signature, and enrichment analyses highlighted IL-1 family, Toll-like receptor, and JAK–STAT signaling pathways. Docking analyses supported high-affinity binding of melittin to IL-1R8 and STAT3, while ADMET profiling suggested limited permeability and low predicted cardiotoxicity.

Conclusion: Melittin exerts a multilayered immunomodulatory effect in SH-SY5Y neuroblastoma cells by activating an IL-37a-centered anti-inflammatory response while suppressing canonical pro-inflammatory signaling pathways.

1. Introduction

Neuroblastoma (NB) is an embryonic malignancy arising from neural crest–derived precursor cells of the sympathetic nervous system and represents the most common extracranial solid tumor in childhood (Feng et al. 2023; Pieniążek et al. 2024). Despite advances in multimodal treatment strategies, NB remains responsible for a substantial proportion of pediatric cancer–related mortality, accounting for approximately 8–10% of all childhood cancers. In high-risk patients, five-year survival rates remain below 50%, largely due to early metastatic dissemination, pronounced biological heterogeneity, and the presence of therapy-resistant phenotypes (Feulefack et al. 2021; Gerges and Canning 2024). These characteristics underscore the urgent need for the development of more effective therapeutic strategies for NB.

Chronic inflammation is a key determinant of tumor initiation, progression, and immune evasion. While acute inflammation supports tissue repair, persistent inflammatory responses lead to reprogramming of

the tumor microenvironment, thereby promoting genomic instability, facilitating immunosuppressive cell infiltration, and triggering the activation of pro-oncogenic signaling pathways such as NF-κB, JNK, and STAT3 (Chavda, Feehan, and Apostolopoulos 2024; Singh et al. 2019). In NB, cytokines including IL-6, IL-10, and TNF-α, secreted by tumor-associated macrophages and infiltrating immune cells, amplify inflammation-driven oncogenic processes and contribute to therapeutic resistance (Sohrab et al. 2023; Tomolonis et al. 2023). Collectively, these findings position NB as an inflammation-associated malignancy and highlight the therapeutic relevance of cytokine-mediated immune regulation.

The IL-1 cytokine family, which plays a central role in the regulation of both innate and adaptive immune responses, occupies a critical position in the control of inflammation in neuroblastoma (NB) (Voronov et al. 2003). Interleukin-37 (IL-37), a unique anti-inflammatory member of this family, exerts broad immunosuppressive effects by inhibiting key inflammatory signaling pathways, including NF-κB, MAPK, and PI3K/AKT/mTOR (Gu et al. 2023; Mei et al. 2020). Notably, the IL-37a isoform is the only variant expressed in the central nervous system, further increasing its relevance in the context of neuro-oncology (Li et al. 2022; Mansour et al. 2021; Wei et al. 2023). Although IL-37 has been reported to exhibit anti-tumor effects in various settings, its functional role and regulatory mechanisms in NB remain largely undefined. Moreover, whether pharmacological agents can modulate IL-37a expression or IL-37-associated signaling networks in NB has not yet been investigated.

Apis mellifera venom represents a rich source of bioactive molecules with therapeutic potential (Khalil et al. 2021). Melittin (MEL), the principal component of bee venom, is an amphipathic α-helical peptide that displays a wide spectrum of anti-cancer activities, including membrane-disruptive, pro-apoptotic, immunomodulatory, and anti-metastatic effects (Haque et al. 2023; Wang et al. 2022). MEL has been shown to

influence multiple oncogenic pathways, such as PI3K/AKT/mTOR, NF-κB, STAT3, and Wnt signaling, disrupt mitochondrial function, increase oxidative stress, and suppress MMP-2/9 and VEGF-mediated angiogenesis, thereby limiting tumor progression(Lee and Bae 2016; Pandey et al. 2023; Pedro et al. 2025). Given the inflammation-driven biology of NB, the combined anti-inflammatory and anti-tumor properties of MEL render it a particularly attractive therapeutic candidate.

Nevertheless, how melittin affects IL-37a expression or IL-37-associated signaling pathways in neuroblastoma remains unknown. This knowledge gap highlights an important area of investigation with translational relevance, offering the potential to uncover a previously unrecognized immunoregulatory mechanism in NB.

Therefore, the present study aims to investigate how melittin modulates IL-37a-associated inflammatory signaling and extracellular matrix (ECM) remodeling pathways in SH-SY5Y neuroblastoma cells. To address this objective, a comprehensive experimental and computational approach was employed, integrating cell viability analysis (MTT assay), gene expression profiling (qRT-PCR), structure-based modeling and molecular docking analyses, together with pathway-level bioinformatics evaluations, including STRING-based protein–protein interaction analysis, Gene Ontology (GO), KEGG pathway

enrichment, and principal component analysis (PCA). Elucidating the molecular mechanisms through which melittin regulates IL-37a-mediated immune modulation is expected to provide a mechanistic framework for evaluating this peptide as a potential immunomodulatory therapeutic candidate in inflammation-driven pediatric cancers.

2. Materials and Methods

2.1. Preparation and Dilution of Melittin

Melittin (CAS No. 20449-79-0) was obtained in lyophilized form from AlfaBioSci (China) with a reported purity of ≥98% (HPLC grade). The peptide was reconstituted in sterile double-distilled water (ddH_2O) to prepare a stock solution and stored at −20°C. Working concentrations (1, 2, 4, 8, 16, and 32 µM) were freshly prepared immediately before each experiment by dilution in complete culture medium.

Exposure Concentration and Duration Justification

The melittin concentrations used in this study (1–32 µM) were selected to encompass a biologically relevant range based on IC_{50} values determined from cell viability assays. This concentration range was chosen to (i) identify the minimum dose associated with a measurable cytotoxic response (IC_{50}), (ii) evaluate dose- and time-dependent transcriptional responses, and (iii) reflect exposure levels commonly employed in mechanistic in vitro studies focusing on intracellular immune and inflammatory signaling rather than systemic toxicity.

Exposure durations of 24 and 48 h were selected to represent early and sustained cellular responses, respectively, thereby enabling the assessment of time-dependent changes in gene expression.

2.2. Cell Lines and Culture Conditions

Human SH-SY5Y (CRL-2266) neuroblastoma cells were obtained from the American Type Culture Collection (ATCC). Cells were cultured in a mixture of Dulbecco's Modified Eagle Medium (DMEM) and Ham's F-12 medium (Capricorn Scientific, Germany) supplemented with 10% fetal bovine serum (FBS; Gibco, USA) and 1% penicillin–streptomycin (50 U/mL penicillin and 50 µg/mL streptomycin; Sartorius, Germany). Cultures were maintained at 37°C in a humidified incubator containing 5% CO_2.

2.3. MTT Cell Viability Assay

SH-SY5Y cells were seeded into 96-well plates at a density of 3 × 10^3 cells per well and exposed to increasing concentrations of melittin for 24 and 48 hours. Subsequently, MTT solution (Biotium, USA) was added, and cells were incubated for an additional 3 hours at 37°C. Formazan crystals were dissolved in isopropanol (Isolab, Germany), and absorbance was measured at 570 nm using a BioTek Epoch 2C microplate reader equipped with Gen5 software. No undissolved formazan crystals were observed during analysis.

Cell viability was calculated by comparing the absorbance values of treated wells with those of

untreated control wells. All experiments were performed in triplicate, and the IC_{50} value was determined based on the 24-hour treatment data.

2.4. RNA Isolation and Quantitative Real-Time PCR Analysis

Total RNA was isolated from each sample using the RiboEx™ RNA Isolation Kit (GeneAll Biotechnology Co., Ltd., Seoul, South Korea) according to the manufacturer's instructions. First-strand complementary DNA (cDNA) was synthesized from 1 µg of total RNA using the A.B.T.™ cDNA Synthesis Kit (Atlas Biotechnology, Ankara, Türkiye) following the kit protocol. The concentration and purity of the synthesized cDNA were assessed using a Qubit™ 2.0 Fluorometer and the Qubit™ ssDNA Assay Kit (Invitrogen, Carlsbad, CA, USA).

Quantitative real-time PCR (qRT-PCR) was performed using SYBR Green Master Mix (A.B.T., Atlas Biotechnology, Ankara, Türkiye) on an Applied Biosystems QuantStudio™ 5 Real-Time PCR System (Applied Biosystems™, Foster City, CA, USA). Each 20 µL reaction mixture contained 10 µL SYBR Green Master Mix, 1 µL forward primer (10 µM), 1 µL reverse primer (10 µM), 2 µL diluted cDNA (1:5), and 6 µL nuclease-free water. All reactions were conducted in triplicate.

PCR cycling conditions consisted of an initial denaturation at 95°C for 5 minutes, followed by 40 cycles of denaturation at 95°C for 15 seconds and annealing/extension at 55°C for 60 seconds. To verify amplification specificity, melt curve analysis was performed from 60°C to 95°C with 0.5°C increments every 5 seconds. Relative gene expression levels were calculated using the $2^{-}\Delta\Delta Ct$ method and normalized to GAPDH expression. Primer sequences are provided in Table 1.

2.5 Heatmap Construction and Principal Component Analysis (PCA)

Multivariate transcriptional analysis was performed using log_2-transformed fold-change values obtained from qRT-PCR experiments. The analysis focused on ten genes associated with inflammation, immune regulation, and extracellular matrix remodeling (IL-37a, IL-18R1, IL-1R8, NF-κB, STAT3, MyD88, Caspase-1, Smad3, MMP-2, and MMP-9). All analyses were conducted using three biological replicates per condition.

A hierarchical clustering heatmap was generated using Heatmapper (https://heatmapper.ca). Pearson correlation was applied as the similarity metric, and complete linkage was used as the clustering method. To emphasize relative differences between experimental conditions, gene expression values were normalized on a row-wise basis.

To evaluate variance structure and treatment-dependent clustering, principal component analysis (PCA) was performed on the log_2-transformed dataset using GraphPad Prism 10. The first two principal components were visualized both as a score plot, illustrating sample separation, and as a biplot displaying gene loadingvectors and their respective contributions to overall variance.

This integrated multivariate approach clearly demonstrated coordinated transcriptional alterations between melittin-treated and control groups, resulting in a robust separation of experimental conditions.

2.6. Bioinformatic Analysis and Pathway Mapping

Transcriptomic data derived from melittin-treated SH-SY5Y cells were analyzed to identify functional pathways and interaction networks. Gene Ontology (GO) and Kyoto Encyclopedia of Genes and Genomes (KEGG) functional annotation and pathway enrichment analyses were performed using the STRING v12.0 platform (https://string-db.org/). GO terms were classified into Biological Process (BP), Cellular Component (CC), and Molecular Function (MF) categories, while KEGG analysis was used to evaluate signaling and regulatory pathways.

Protein–protein interaction (PPI) networks were constructed in STRING using a high-confidence interaction threshold (confidence score > 0.7). Enrichment significance was assessed using a false discovery rate (FDR)-adjusted p-value cutoff of < 0.05. GO and KEGG enrichment bubble plots, as well as STRING clustering maps, were exported for visualization using *Homo sapiens* as the background reference. All gene nomenclature follows HGNC standards, as detailed in Table 2.

2.7. Protein Preparation

The molecular structure of melittin was retrieved from the RCSB Protein Data Bank (PDB ID: 2MLT), while the corresponding predicted model was obtained from the AlphaFold Protein Structure Database (UniProt ID: P01501). Prior to analysis, both structures were prepared using Discovery Studio 2021. This preparation included the removal of crystallographic water molecules, addition of hydrogen atoms, and optimization of bond geometries and side-chain conformations.

For structural comparison, the experimental melittin structure (PDB: 2MLT) and the AlphaFold-predicted model (UniProt: P01501) were analyzed using UCSF Chimera (version 1.19.1, build 44171). Structural similarity, amino acid sequence alignment, and AlphaFold confidence metrics, including per-residue pLDDT scores, were evaluated to assess model reliability.

In addition, a two-dimensional chemical structure illustrating the amino acid composition and peptide backbone connectivity of melittin was generated based on the molecular representation provided by the Mcule 1-Click Docking tool and included as part of the analysis.

2.8. Protein and Ligand Preparation for Molecular Docking

The three-dimensional structure of melittin was retrieved from the RCSB Protein Data Bank (PDB ID: 2MLT). The crystal structures of the target proteins STAT3 (PDB ID: 6NJS) and IL-1R8 (SIGIRR) (PDB ID: 6D65) were also obtained from the RCSB Protein Data Bank. All structures were prepared using UCSF Chimera (version 1.19.1).

Protein and ligand preparation steps included the removal of crystallographic water molecules, addition of hydrogen atoms, assignment of Kollman charges, and optimization of side-chain conformations when required. Energy minimization and structural refinement were performed using the “DockPrep” tool and the “Minimize Structure” function implemented in Chimera. The prepared melittin structure was subsequently saved in PDB format for use in downstream docking analyses.

Protein–protein docking simulations between melittin (ligand) and STAT3 or IL-1R8 (receptors) were performed using the HDOCK server (http://hdock.phys.hust.edu.cn/) with default parameters. HDOCK conducts a global docking search and ranks predicted complexes based on an integrated scoring function. For each interaction, the top ten predicted docking models were evaluated. The model with the most favorable docking score and the highest confidence score was selected as the representative binding pose. Docking scores, confidence scores, and ligand RMSD values were recorded from the server output for further analysis.

2.9. In Silico ADMET Prediction

The ADMET (Absorption, Distribution, Metabolism, Excretion, and Toxicity) properties of melittin were predicted using the online ADMETlab 3.0 platform (https://admetmesh.scbdd.com/). The canonical SMILES representation of melittin was used as the input. The platform generated a multiparametric profile by estimating physicochemical properties, medicinal chemistry parameters, pharmacokinetic characteristics, and multiple toxicity endpoints to assess the drug-likeness and potential safety liabilities of the peptide.

2.10. Statistical Analysis

Data obtained from at least three independent experiments ($n \geq 3$) were expressed as mean ± standard deviation (SD). Statistical analyses of experimental data, including MTT and qRT-PCR results, were performed using GraphPad Prism software (version 10.0). Normality of data distribution was assessed using the Shapiro–Wilk test.

Comparisons between two groups were conducted using an unpaired, two-tailed Student’s *t*-test. For analyses requiring multiple comparisons against a single control group (e.g., MTT dose–response experiments), one-way analysis of variance (one-way ANOVA) was applied. A p value < 0.05 was considered statistically significant. Levels of significance were denoted as $p < 0.05$, $*p < 0.01$, $**p < 0.001$, and $***p < 0.0001$.

For *in silico* analyses, the top-ranked docking models generated by the HDOCK server were selected based on the most favorable docking score and confidence score according to the server’s internal ranking system. Gene Ontology (GO) and KEGG enrichment analyses obtained from the STRING platform were considered statistically significant at a false discovery rate (FDR)–adjusted p value < 0.05. ADMET predictions were reported as generated by the ADMETlab 3.0 platform, and no additional statistical analyses were applied.

3. Results

3.1. Melittin Reduces the Viability of SH-SY5Y Neuroblastoma Cells

To evaluate the cytotoxic effect of melittin, SH-SY5Y neuroblastoma cells were treated with increasing concentrations of melittin (1, 2, 4, 8, 16, and 32 μM) for 24 and 48 hours, and cell viability was assessed using the MTT assay. After 24 hours of treatment, melittin induced a dose-dependent reduction in cell viability, with viability falling below 50% for the first time at concentrations of 16 μM and above ($p < 0.0001$) (Figure 1A). At 48h, the cytotoxic effect became more pronounced, and cell viability dropped below 50% at concentrations above 4 μM, indicating an increased dose- and time-dependent cellular sensitivity to melittin (Figure 1B).

Although a reduction in viability was observed at both time points, the IC_{50} value was calculated using the 24-hour data to reflect the earliest measurable cytotoxic response. Statistical analysis performed using GraphPad Prism 10confirmed a significant decrease in cell viability in all melittin-treated groups compared with the control group (Figure 1A). According to the AAT Bioquest IC_{50} Calculator, the IC_{50} value of melittin at 24 hours was determined to be 16 μM (Figure 1C).

To support the MTT findings, cell morphology was examined under a brightfield microscope. SH-SY5Y cells treated with melittin at the IC_{50} concentration for 24 hours exhibited reduced cell density, disruption of membrane integrity, and retraction of neurite-like extensions, indicating pronounced cytotoxic and morphological alterations compared with control cells (Figure 1D).

3.2. Melittin Induces an IL-37a–Centered Anti-Inflammatory Transcriptional Response in SH-SY5Y Cells

To investigate the transcriptional effects of melittin in SH-SY5Y neuroblastoma cells, RT–qPCR analysis was performed for genes associated with inflammation, immune signaling, and extracellular matrix (ECM) remodeling. Gene expression levels were normalized to the housekeeping gene β-actin (ACTB), and fold changes were calculated using the $2^{-}\Delta\Delta Ct$ method.

Melittin treatment resulted in a significant upregulation of IL-37a ($p < 0.001$) and IL-18R1 ($p < 0.05$), indicating activation of an IL-37a-mediated anti-inflammatory cytokine response (Figures 2A–B). In addition, expression of IL-1R8 (SIGIRR), a negative regulator of IL-1 family signaling, was significantly increased following melittin exposure ($p< 0.05$) (Figure 2C). These findings suggest that melittin enhances cytokine signaling modulation through activation of the IL-37a–IL-1R8 axis. Consistently, the pro-inflammatory transcription factor NF-κB was significantly downregulated ($p < 0.01$), supporting an inhibitory effect of melittin on pro-inflammatory signaling (Figure 2D).

Analysis of intracellular inflammatory regulators revealed a significant increase in Caspase-1 expression ($p < 0.01$) following melittin treatment (Figure 2G). In contrast, key signal transducers involved in innate immune and inflammatory pathways—MyD88 ($p < 0.05$), STAT3 ($p < 0.01$), and Smad3 ($p < 0.001$)—were significantly downregulated (Figures 2E, 2F, and 2H).

Melittin treatment elicited a differential response in genes associated with ECM remodeling. While MMP-2 expression was significantly upregulated ($p < 0.001$), MMP-9 levels were markedly reduced ($p < 0.001$) (Figures 2I–J), indicating gene-specific modulation of matrix remodeling processes.

Global assessment of gene expression profiles using hierarchical clustering heatmap analysis (Figure 2K) demonstrated a clear separation between control and melittin-treated samples, revealing a coordinated transcriptional reprogramming involving inflammatory, cytokine-regulatory, and ECM-related genes.

Overall, these results demonstrate that melittin strengthens an IL-37a-centered anti-inflammatory response in SH-SY5Y neuroblastoma cells, suppresses major pro-inflammatory signaling components such as NF-κB, MyD88, STAT3, and Smad3, and differentially regulates ECM remodeling factors, highlighting its multifaceted immunomodulatory effects.

3.3. Melittin Alters Gene Expression Patterns Consistent with IL-37–Associated Immune Regulation

To obtain an integrated view of the transcriptional response to melittin, hierarchical clustering and principal component analysis (PCA) were applied to a qRT–PCR dataset comprising ten genes associated with inflammation, immune regulation, and extracellular matrix remodeling.

The hierarchical clustering heatmap (Figure 3A) revealed a clear separation between control and melittin-treated groups. The tight clustering of melittin-treated samples into a single cluster indicates a coordinated transcriptional shift involving components of the IL-37a/IL-1R8 axis, intracellular signaling regulators, and matrix remodeling genes. The distinct clustering of control samples further supports the notion that melittin induces a treatment-specific and structurally organized gene expression program.

This separation was further reinforced by the PCA score plot (Figure 3B). The first principal component (PC1) accounted for 89.48% of the total variance, while the second principal component (PC2) explained 5.24%. Melittin-treated samples clustered in the positive region along PC1, whereas control samples were located in the negative region, with no overlap observed between the two groups. This pronounced segregation demonstrates that melittin elicits a robust, stable, and treatment-specific transcriptional signature in SH-SY5Y cells.

The PCA biplot (Figure 3C) identified the genes contributing most strongly to this separation. IL-37a, IL-1R8, IL-18R1, Caspase-1, and MMP-2 showed positive loadings associated with melittin treatment and contributed substantially to the separation of melittin-treated samples along the PC1 axis. In contrast, NF-κB, STAT3, MyD88, Smad3, and MMP-9were oriented toward the control cluster, confirming their downregulation by melittin. This distribution indicates that melittin enhances an IL-37-centered immunoregulatory response while concomitantly attenuating canonical pro-inflammatory signaling pathways.

Overall, these multivariate analyses demonstrate that melittin drives a structured and treatment-specific gene expression program in SH-SY5Y neuroblastoma cells, characterized by activation of IL-37-

associated immune modulation and coordinated suppression of pro-inflammatory signaling pathways.

3.4. STRING Network, GO/KEGG Annotation, and Enrichment Analysis of Melittin-Induced Neuroinflammatory Signaling

To elucidate the potential biological functions and pathway-level organization of genes regulated by melittin, STRING-based protein–protein interaction (PPI) analysis, Gene Ontology (GO) annotation, and KEGG pathway enrichment profiling were performed.

The STRING PPI network (Figure 4A) revealed a highly interconnected interaction map among the analyzed genes. STAT3, NFKB1, MYD88, SMAD3, and CASP1 occupied central positions within the network, indicating their roles as key signaling hubs, while MMP2 and MMP9 were also integrated into the interaction framework. In contrast, IL37, IL18R1, and SIGIRR were positioned as higher-order regulatory nodes, consistent with their immunomodulatory functions.

The STRING local cluster enrichment analysis (Figure 4B) further supported these observations, demonstrating significant enrichment of processes related to the IL-1 cytokine family, Toll-like receptor signaling, cytokine–receptor interactions, and the JAK–STAT signaling cascade.

Evaluation of KEGG pathway enrichment analyses, based on both statistical significance (Figure 4C) and gene contribution counts (Figure 4E), highlighted the prominence of cytokine–cytokine receptor interaction pathways, inflammation-associated signaling pathways, and immune response–related cancer pathways.

Similarly, GO Biological Process enrichment, assessed according to −log(FDR) ranking (Figure 4D) and gene distribution patterns (Figure 4F), confirmed that melittin predominantly modulates biological processes associated with inflammation, cytokine production, immune activation, and cellular stress adaptation.

Collectively, these analyses demonstrate that melittin activates a multilayered and coordinated neuroinflammatory transcriptional program in SH-SY5Y neuroblastoma cells, encompassing not only differential gene expression but also integrated regulation of inflammatory signal transduction, stress adaptation mechanisms, and extracellular matrix remodeling.

3.5. Structural Comparison of Experimental and Predicted Melittin Models

To assess the conformational reliability of the artificial intelligence–predicted melittin model, the experimentally determined crystal structure (PDB ID: 2MLT) was compared with the AlphaFold-predicted model (UniProt ID: P01501). Both structures exhibited a conserved α-helical conformation spanning residues 5–21, corresponding to the core functional region of the peptide (Figures 5A–B).

In both models, the N-terminal segment displayed partial structural disorder, whereas the C-terminal tail exhibited variable flexibility, consistent with previously reported structural dynamics of melittin.

The pLDDT confidence score profile of the AlphaFold model further supported these observations, showing high per-residue confidence values within the central helical region, while the terminal regions displayed lower scores, reflecting inherent conformational mobility.

Overall structural alignment revealed no significant deviations between the experimental and predicted models in terms of helix orientation, backbone topology, or residue packing. These findings confirm that the AlphaFold-generated structure accurately represents the biologically relevant conformation of melittin and is therefore suitable for molecular docking studies and protein–ligand interaction analyses, particularly those focusing on the stable helical core of the peptide (Figure 5C).

3.6. Molecular Docking Analysis Reveals High Binding Affinity of Melittin to STAT3 and IL-1R8

To elucidate potential direct interactions between melittin and key signaling proteins involved in IL-37a–associated pathways, molecular docking simulations were performed against STAT3 and IL-1R8 (SIGIRR).

Docking results demonstrated an exceptionally strong theoretical binding affinity between melittin and IL-1R8. The top-ranked docking model achieved a docking score of −296.74 with a confidence score of 0.9495 (Figure 6A, Table 1). Similarly, docking analysis against STAT3 revealed a robust interaction, with the best-scoring model exhibiting a docking score of −200.27 and a confidence score of 0.7321 (Figure 6B, Table 3).

These high docking scores indicate that melittin has the potential to directly bind critical nodal proteins within the inflammatory signaling network, providing a structural basis for the experimentally observed modulation of IL-37a–associated pathways.

3.7. In Silico ADMET Profiling Reveals the Drug-Likeness Characteristics of Melittin

Given the promising anticancer activity of melittin, its pharmacokinetic and toxicological profile was evaluated using the ADMETlab 3.0 platform to assess its potential as a therapeutic lead compound (Table 4).

The analysis revealed both strengths and challenges associated with the peptide nature of melittin (Figure 7). As a 26–amino acid peptide, melittin exhibits a high molecular weight (2844.75 Da) and elevated numbers of hydrogen bond donors and acceptors (nHD = 50, nHA = 70), placing it outside the optimal ranges defined by conventional small-molecule drug-likeness rules (e.g., Lipinski, Pfizer), which is consistent with a predicted low oral bioavailability. These findings were further supported by low predicted Caco-2 and MDCK permeability scores. In addition, melittin was predicted to act as a P-glycoprotein inhibitor and to possess a very low free plasma fraction (Fu = 133.67%), indicating a strong tendency for plasma protein binding.

Notably, melittin was predicted to have a low probability of hERG channel blockade (cardiotoxicity risk) and drug-induced liver injury (DILI). However, alerts were identified for potential nephrotoxicity,

ototoxicity, and neurotoxicity, which are consistent with known safety concerns associated with cytotoxic peptides. The high synthetic accessibility score (9.0) further suggests that chemical synthesis of melittin may be challenging.

In summary, although melittin demonstrates potent biological activity, its ADMET profile highlights significant limitations for systemic administration arising from its peptide structure, underscoring the need for specialized formulation strategies or localized delivery approaches to enable its therapeutic application.

4. Discussion

Neuroblastoma is a therapeutically challenging malignancy in pediatric oncology. Inflammatory signaling pathways play a critical role in disease progression, underscoring the need for novel therapeutic strategies that specifically target these processes. Melittin, a major bioactive component of *Apis mellifera* venom, is a peptide that has been reported to exhibit both anti-inflammatory and anticancer properties across multiple cancer types (Ağan and Kekeçoğlu 2020; Wang et al. 2022). However, the effects of melittin on neuroblastoma cells—particularly with respect to IL-37a-associated immunoregulatory mechanisms—remain largely undefined. The present study demonstrates that melittin exerts pronounced antitumor effects in SH-SY5Y neuroblastoma cells. Our findings provide *in vitro* and in silico evidence indicating that melittin upregulates IL-37a expression and modulates molecular pathways associated with this anti-inflammatory axis.

To evaluate the cytotoxic effects of melittin in SH-SY5Y neuroblastoma cells, cells were treated with increasing concentrations of melittin, and cell viability was assessed using the MTT assay. Melittin induced dose-dependent cytotoxicity at both 24 and 48 hours of incubation. At 24-hour time point, cell viability declined below 50% for the first time at concentrations of 16 μM and above, and to capture this early cytotoxic response, the IC_{50} value was calculated using 24-hour data, yielding an IC_{50} of 16 μM. At 48 hours, increased cellular sensitivity to melittin was observed, with greater than 50% loss of viability at concentrations above 4 μM, indicating a clear time-dependent enhancement of cytotoxicity.

As no previous studies have reported IC_{50} values for melittin in SH-SY5Y cells, our work provides one of the first quantitative cytotoxicity profiles for this neuroblastoma cell line. Comparative analysis with other neuroectodermal tumor models suggests that SH-SY5Y cells are relatively more resistant to melittin at early exposure times. For example, IC_{50} values of approximately 1–2 μM have been reported in LA-N-1 neuroblastoma cells after 4 hours of treatment (Drechsler and Andrä 2011), while glioblastoma-derived LN229 (≈3 μM) and LN18 (≈6 μM) cells exhibited cytotoxic responses only after 72 hours of incubation (Wang et al. 2024). In contrast, our results show that prolonged exposure markedly increases melittin sensitivity in SH-SY5Y cells, with substantial loss of viability at 48 hours even at lower concentrations. These findings indicate that although SH-SY5Y cells display relative resistance to melittin at shorter incubation periods, melittin sensitivity increases significantly with extended exposure, consistent with previously reported time-dependent cytotoxic profiles.

It is noteworthy that, in the literature, melittin is generally effective in epithelial tumors at lower IC_{50} values. In particular, high cytotoxicity of melittin has been reported in colorectal cancer cells (HCT116; 3.8 μM, 24 h) (Zamani, Bozorg-Ghalati, and Mokarram 2024), ovarian cancer cells (SKOV3; ≈2 μM, 24 h) (Wu et al. 2025), prostate cancer cells (DU145; 1.7 μM, LNCaP 1.8 μM, 48 h) (Yan et al. 2023) and in certain lung cancer models (A549; 50 μM, 24 h) (Ibrahim et al. 2025). In hematological malignancies, this effect appears to be even more pronounced; notably, IC_{50} values in K-562 leukemia cells have been reported to decrease to 1–2 μMfollowing 96 h of incubation (Obeidat et al. 2023). These findings indicate that melittin generally exhibits a stronger cytotoxic profile in epithelial and hematological cancer cells, whereas the IC_{50} value obtained in SH-SY5Y neuroblastoma cells in the present study (16 μM, 24 h) is relatively higher, reflecting cell type–dependent differences in sensitivity.

The wide range of IC_{50} values reported in the literature across different cancer types cannot be explained solely by cell type–specific biological responses; rather, the source, purity, and preparation methods of the melittin used also play an important role in this variability. Melittin manually purified from bee venom may contain varying proportions of other peptides and enzymes, which can differentially affect cellular metabolism and, consequently, lead to substantial inter-laboratory variability in IC_{50} values. In contrast, commercially synthesized melittin, owing to its high purity and batch-to-batch standardization, yields more reproducible and directly comparable results. Therefore, the interpretation of the IC_{50} value obtained in the SH-SY5Y cell line critically depends on the source of melittin used, and comparisons with other IC_{50} values reported in the literature should be made with careful consideration of these methodological differences. In this context, the use of high-purity melittin in the present study indicates that the observed cytotoxicity profile is reliable and reproducible.

The therapeutic potential of melittin in cancer treatment is not limited to its cytotoxic effects but also derives from its impact on molecular mechanisms regulating inflammation and tumor progression. Chronic inflammation is known to facilitate tumor development by creating a supportive microenvironment that promotes cell proliferation, invasion, and immune evasion. Therefore, the modulation of inflammatory responses and the integration of inflammation-regulating molecules such as MEL into therapeutic strategies represent a compelling approach in cancer biology. In this context, the present study investigated the effects of MEL on gene expression associated with IL-37a and related signaling pathways.

Interleukin-37 (IL-37) is a relatively recently characterized regulatory cytokine that is exclusively expressed in humans and exists in five isoforms (IL-37a–e) (Wei et al. 2023). Among these isoforms, IL-37a has been identified as a potent anti-inflammatory cytokine acting as a negative regulator of inflammation and plays a critical role in suppressing the tumor microenvironment (Gu et al. 2023). IL-37a inhibits pro-inflammatory and tumor-promoting cytokines such as IL-6, TNF-α, and IL-1β, thereby suppressing pro-tumorigenic signaling pathways including PI3K/AKT/mTOR and STAT3 (Li et al. 2022; Mansour et al. 2021). It has also been shown to downregulate the expression of metastasis-associated matrix metalloproteinases MMP-2 and MMP-9 (Huang et al. 2021). These pleiotropic regulatory effects

position IL-37a as a strong candidate for next-generation therapeutic strategies targeting the immune and inflammatory components of cancer.

To date, no studies have been reported in the literature investigating the effects of melittin on an interleukin with anti-cancer and anti-inflammatory properties such as IL-37a. This gap clearly highlights the need for studies examining the potential effects of MEL on IL-37a-associated immune and inflammatory regulatory mechanisms.

Within the scope of the present study, the gene expression levels of IL-37a, IL-1R8 (SIGIRR), and IL18R1 were compared between MEL-treated and untreated SH-SY5Y cells. Compared with the control group, MEL-treated cells exhibited a 2.85-fold increase in IL-37a expression ($p < 0.001$), a 1.80-fold increase in IL-1R8 (SIGIRR) expression ($p < 0.05$), and a 0.88-fold increase in IL18R1 expression ($p < 0.05$). These findings suggest that melittin is capable of significantly modulating the IL-37a-associated immunoregulatory axis.

Extracellular IL-37 forms a tripartite receptor complex with IL-18Rα and IL-1R8 (SIGIRR), which plays a critical role in regulating downstream signaling pathways such as STAT3 and PTEN. This receptor complex has been defined as a fundamental mechanism not only for the suppression of inflammatory responses but also for the modulation of cell proliferation and survival signaling (Mei and Liu 2019). STAT3 is a central transcription factor governing proliferation, survival, metastasis, and angiogenesis, and its aberrant activation is widely recognized as a key driver of tumor progression (Hu, Dong, and Liu 2024). The study by Jo et al. demonstrated that bee venom and melittin dose-dependently reduced STAT3 levels in ovarian cancer cells (Jo et al. 2012). These findings indicate that inhibition of STAT3 activity by melittin may represent an important mechanism underlying its tumor growth– and metastasis-limiting effects.

When evaluated in light of this literature, the 0.54-fold suppression of STAT3 expression following MEL treatment in our study ($p < 0.01$) is fully consistent with the reported antitumoral effects of melittin mediated through inhibition of the JAK2/STAT3 signaling pathway. This pronounced reduction in STAT3 levels suggests that melittin may exert antineoplastic effects in SH-SY5Y cells by attenuating proliferation and survival responses. Accordingly, STAT3 inhibition emerges as one of the principal mechanisms through which melittin modulates cellular responses.

MMPs play a central role in cancer metastasis by regulating multiple biological processes, including the tumor microenvironment, cell adhesion, migration, and invasion. In particular, MMP-2 and MMP-9are critical enzymes that enable tumor cells to breach tissue barriers and disseminate to distant organs. The effects of IL-37 on the MMP family have been reported to be context-dependent, with marked suppression of MMP-2 and MMP-9 observed predominantly within the tumor microenvironment, while these effects may be more limited in tumor cells themselves (Reddy, Sai Varshini, and Kumar 2023; Shoari, Coban, and Radisky 2025). Indeed, Mei et al. demonstrated that IL-37 did not directly reduce MMP-2 expression in SK-Hep-1 and SMMC-7721 cells; however, it significantly decreased the expression of both MMP-2 and MMP-9 in the peritumoral region (Mei et al. 2020). Similarly, Huang et al. reported

that melittin strongly reduced MMP-2 and MMP-9 expression as well as gelatinase activity in AGS cells, suggesting that melittin may exert anti-metastatic effects by suppressing extracellular matrix degradation and invasive capacity (Huang et al. 2021).

It is well established that the transcriptional activity of matrix metalloproteinases (MMPs) is largely regulated by NF-κB–dependent signaling pathways. Cho et al. reported that bee venom strongly inhibited MMP-9 expression in PMA-stimulated MCF-7 cells via JNK/p38 MAPK signaling, predominantly through NF-κB–dependent mechanisms (Cho et al. 2010). Considering that NF-κB is one of the principal transcriptional regulators of the MMP-9 promoter, these findings suggest that melittin may limit metastatic behavior by suppressing this pathway [35].

In addition, Sun et al. demonstrated that melittin reduces MMP-9 expression not only through NF-κB inhibition but also via suppression of the JAK2–STAT3 signaling pathway (Sun et al. 2025). The pronounced reduction of p-JAK2, p-STAT3, and MMP-9 levels by melittin in both *in vitro* and *in vivo* models indicates that STAT3 may function as a second transcriptional regulatory axis for MMP-9, operating in parallel with NF-κB. Consistent with these literature findings, our study demonstrated a 1.98-fold decrease in MMP-9 expression following MEL treatment ($p < 0.001$), accompanied by a 2.61-fold suppression of NF-κB expression ($p < 0.01$). In contrast, MMP-2 expression was significantly increased by 1.95-fold ($p < 0.001$). Taken together, these data indicate that melittin suppresses the IL-37a–NF-κB–MMP-9 axis in SH-SY5Y cells, thereby eliciting anti-inflammatory and anti-metastatic responses, while MMP-2 appears to be regulated through alternative pathways independent of IL-37 signaling.

MyD88 is a central adaptor molecule mediating signals transmitted by members of the IL-1 receptor family, particularly through IL-18R, and plays a critical role in the regulation of inflammatory responses. Accordingly, the IL-18R–MyD88 axis is regarded as a key component of intracellular inflammatory signal transduction. Although no studies have directly investigated the effects of melittin on MyD88 in the context of cancer, evidence from different experimental models suggests that melittin may influence MyD88-dependent signaling pathways. For instance, Yao et al. reported that melittin attenuated the TLR4–MyD88–NF-κB signaling axis in an ischemic stroke model (Yao et al. 2024). In addition, Güneş et al. demonstrated that oleandrin treatment reduced MyD88 expression in melanoma cells, indicating that certain natural compounds are capable of modulating MyD88-associated inflammatory pathways (Eroğlu Güneş et al. 2022).

Furthermore, a study by Palm et al. revealed that MyD88 is involved not only in TLR–IL-1R–mediated signaling but also in the broader regulation of inflammatory cellular responses (Palm et al. 2013). Taken together, these findings suggest that the suppressive effect of melittin on NF-κB signaling may be associated with a reduction in upstream MyD88-mediated signaling events. Consistent with this mechanistic framework, our study demonstrated a 0.61-fold decrease in MyD88 expression following MEL treatment ($p < 0.05$). Nevertheless, further studies are required to elucidate the precise molecular mechanisms through which melittin modulates MyD88 expression and signaling in SH-SY5Y neuroblastoma cells.

Caspase-1 is a critical protease that plays a central role in the regulation of inflammatory responses by mediating the maturation of the major pro-inflammatory cytokines IL-1β and IL-18 (Sollberger et al. 2014). Lee et al. demonstrated that bee venom–derived superoxide dismutase 3 (bvSOD3) triggers inflammasome activation through excessive H_2O_2 production, resulting in a caspase-1–dependent inflammatory response and cell death (Lee et al. 2022). In addition, Zhao et al. reported that melittin can enhance the antitumor efficacy of molecularly targeted therapies by activating caspase-1–mediated inflammatory signaling (Zhao et al. 2022). Consistent with these findings, our study demonstrated a 1.30-fold increase in caspase-1 expression in SH-SY5Y cells following MEL treatment ($p < 0.01$).

Beyond extracellular IL-18Rα–mediated signaling, the anti-inflammatory functions of IL-37 are also associated with intracellular mechanisms involving direct interaction with SMAD3, leading to suppression of inflammatory gene expression. In a study by Seung-Heon Shin et al., melittin treatment was shown to inhibit SMAD3 signaling, resulting in a significant reduction in SMAD3 activation (Li et al. 2025). In agreement with these observations, our results revealed that SMAD3 expression decreased to 0.77-fold following MEL treatment, and this reduction was statistically significant ($p < 0.001$).

Taken together, these findings indicate that MEL acts in SH-SY5Y cells not only as a cytotoxic agent but also as an effective molecular modulator capable of regulating IL-37a–associated signaling pathways that shape inflammation and the tumor microenvironment.

Transcriptomic analysis demonstrated that melittin induces a distinct and treatment-specific gene expression profile in SH-SY5Y cells. When evaluated in combination with qRT-PCR data, hierarchical clustering, and PCA analyses, melittin treatment was shown to initiate a coordinated transcriptional reprogramming involving the IL-37a/IL-1R8 axis, intracellular signaling regulators, and genes associated with extracellular matrix remodeling.

STRING-based PPI analysis revealed that key genes central to inflammation and immune responses—STAT3, NF-κB, MYD88, SMAD3, and CASP1—form critical network hubs, whereas IL37, IL18R1, and SIGIRR occupy higher-order regulatory positions within the interaction network. This network architecture suggests that the effects of melittin are not random but are instead organized around defined immune and inflammatory signaling pathways.

GO and KEGG enrichment analyses further demonstrated that melittin predominantly modulates cytokine–receptor interactions, innate immune signaling, the JAK–STAT cascade, inflammatory responses, and immune-related cancer pathways. When considered alongside the suppression of NF-κB, STAT3, MyD88, Smad3, and MMP-9, these findings support the conclusion that melittin attenuates pro-inflammatory and tumor-supportive signaling while simultaneously strengthening IL-37–associated

immunoregulatory mechanisms.

Overall, these multilayered analyses demonstrate that melittin does not merely exert cytotoxic effects in SH-SY5Y cells; rather, it activates a structured transcriptional program encompassing immune

regulation, control of inflammation, stress adaptation, and extracellular matrix remodeling. This holistic effect profile supports the consideration of melittin as a potential complementary molecular modulator in inflammation-based cancer therapies.

To establish a link between transcriptional alterations and direct molecular interactions, a computational approach was employed. The high degree of structural similarity between the experimentally determined melittin structure and the AlphaFold-predicted model confirmed the suitability of the predicted structure for reliable docking studies. Molecular docking simulations revealed strong theoretical binding affinities between melittin and two key signaling proteins, IL-1R8 and STAT3. The exceptionally high docking and confidence scores obtained for the melittin–IL-1R8 complex indicate a stable interaction, suggesting that this binding may stabilize the negative regulatory function of IL-1R8. Favorable docking results with STAT3 further suggest that melittin may directly modulate STAT3 activity, potentially diverting it from its canonical oncogenic role or facilitating non-canonical signaling pathways. Collectively, these in silico findings provide a plausible structural mechanism supporting our experimental observations and suggest that melittin may directly target core components of the IL-37a–associated signaling network.

Finally, in silico ADMET profiling provided important insights into the therapeutic potential of melittin. Owing to its nature as a natural peptide, melittin exhibits properties that substantially deviate from those of conventional small-molecule drugs. Its high molecular weight, excessive numbers of hydrogen bond donors and acceptors, and low predicted permeability and oral bioavailability indicate significant delivery challenges for systemic administration. Nevertheless, the predicted low risk of hERG channel blockade and drug-induced liver injury (DILI) is encouraging from a safety perspective. Predicted warnings for nephrotoxicity, ototoxicity, and neurotoxicity are consistent with known dose-limiting toxicities of cytotoxic peptides and underscore the potential necessity of targeted delivery strategies, such as nanoparticle encapsulation or tumor-targeted ligand conjugation, to minimize off-target effects.

5. Conclusion

This study investigated the effects of melittin on neuroblastoma cells using an integrated experimental and bioinformatic approach. Our findings demonstrate that melittin (MEL) exerts dose- and time-dependent cytotoxic effects in SH-SY5Y neuroblastoma cells. Beyond its direct cytotoxic activity, MEL significantly upregulated the IL-37a–associated immunoregulatory axis, including IL-37a, IL-1R8, and IL-18R1, while concurrently suppressing key pro-tumorigenic and pro-inflammatory signaling components, such as STAT3, NF-κB, MyD88, SMAD3, and MMP-9.

In addition, the observed increase in caspase-1 expression, together with coordinated transcriptional changes, suggests that MEL may influence inflammation-associated cell death pathways. Transcriptomic analyses, combined with PPI network construction and GO/KEGG enrichment profiling, revealed that MEL predominantly modulates biological processes related to cytokine signaling, innate immune responses, JAK–STAT pathways, and extracellular matrix organization. Furthermore, molecular

docking analyses demonstrated that MEL exhibits strong binding affinities to IL-1R8 and STAT3, providing a structural basis for the immunomodulatory effects observed at the transcriptional level.

In conclusion, these findings indicate that MEL acts as a dual-function molecule in neuroblastoma, displaying both cytotoxic and immunomodulatory properties, and support its consideration as a promising lead compound for inflammation-based therapeutic strategies. Future studies should focus on validating these interactions in in vivo models and on developing targeted delivery systems to enhance the specificity and safety of MEL, thereby facilitating a clearer assessment of its clinical application potential.

Abbreviations

Abbreviation	Full Term
3D	Three-Dimensional
ADMET	Absorption, Distribution, Metabolism, Excretion and Toxicity
ANOVA	Analysis of Variance
ATCC	American Type Culture Collection
bp	Base Pair
CASP1	Caspase-1
cDNA	Complementary DNA
DEGs	Differentially Expressed Genes
DMEM	Dulbecco's Modified Eagle Medium
DMSO	Dimethyl Sulfoxide
ECM	Extracellular Matrix
FBS	Fetal Bovine Serum
GAPDH	Glyceraldehyde-3-Phosphate Dehydrogenase
GO	Gene Ontology
hERG	Human Ether-à-go-go-Related Gene
IC_{50}	Half-Maximal Inhibitory Concentration
IL-37a	Interleukin-37 alpha
IL-18R1	Interleukin-18 Receptor 1
IL-1R8 (SIGIRR)	Interleukin-1 Receptor 8
JAK	Janus Kinase
KEGG	Kyoto Encyclopedia of Genes and Genomes
MEL	Melittin
MF	Molecular Function
MMP-2	Matrix Metalloproteinase-2
MMP-9	Matrix Metalloproteinase-9
MTT	3-(4,5-Dimethylthiazol-2-yl)-2,5-diphenyltetrazolium bromide
MyD88	Myeloid Differentiation Primary Response 88
NB	Neuroblastoma

NF-κB	Nuclear Factor Kappa B
PBS	Phosphate-Buffered Saline
PCA	Principal Component Analysis
PDB	Protein Data Bank
PI3K	Phosphoinositide 3-Kinase
pLDDT	Predicted Local Distance Difference Test
PPI	Protein–Protein Interaction
qRT-PCR	Quantitative Real-Time Polymerase Chain Reaction
RNA	Ribonucleic Acid
RMSD	Root-Mean-Square Deviation
SD	Standard Deviation
SH-SY5Y	Human Neuroblastoma Cell Line
SMAD3	Mothers Against Decapentaplegic Homolog 3
STAT3	Signal Transducer and Activator of Transcription 3
SYBR	DNA-Binding Fluorescent Dye (SYBR Green)
TLR	Toll-Like Receptor
UCSF	University of California, San Francisco
UniProt	Universal Protein Resource

Declarations

Author Contributions: B.E. Writing – original draft, Visualization, Software, Methodology, Investigation, Formal analysis, Data curation. **T.Y.** Writing – original draft, Visualization, Software, Methodology, Investigation, Formal analysis, Conceptualization**. E.E.** Writing – review & editing, Visualization, Software, Methodology, Investigation, Formal analysis, Data curation. **A.C.** Writing – review & editing, Validation, Supervision, Conceptualization.

Funding: This article is extracted from Berkay Ertan's master dissertation entitled "Melittin's Effect on IL-37 and Associated Pathway Gene Expression Levels in Neuroblastoma Cell Line", supervised by Prof. Dr. Ahmet Carhan (Ph.D. Dissertation, Ankara Yildirim Beyazit University, Ankara, 2025). This research was funded by Ankara Yildirim Beyazit University Research Foundation Project (Ankara, Türkiye) through grant TYK-2024-2642. The authors declare that no funds were available for APC.

Informed Consent Statement: Not applicable.

Data Availability Statement: The data supporting the findings of this study are available from the corresponding author upon reasonable request.

Acknowledgments: During the preparation of this research, the authors utilized multiple AI tools including OpenAI's ChatGPT, Google's Gemini, and DeepSeek for text editing and language enhancement. Following the use of these tools, the authors reviewed and edited the content as necessary and take full responsibility for the final publication.

Conflicts of Interest: The authors declare no conflict of interest.

References

1. Ağan, Aydan Fülden, and Meral Kekeçoğlu. 2020. “Melittin ve Kanser Tedavisi: Nanoteknolojik Bakış Açısı.” *Uludağ Arıcılık Dergisi* 20(2):221–31. doi:10.31467/uluaricilik.784365.
2. Chavda, Vivek P., Jack Feehan, and Vasso Apostolopoulos. 2024. “Inflammation: The Cause of All Diseases.” *Cells* 13(22):1906. doi:10.3390/cells13221906.
3. Cho, Hyun-Ji, Yun-Jeong Jeong, Kwan-Kyu Park, Yoon-Yub Park, Il-Kyung Chung, Kwang-Gill Lee, Joo-Hong Yeo, Sang-Mi Han, Young-Seuk Bae, and Young-Chae Chang. 2010. “Bee Venom Suppresses PMA-Mediated MMP-9 Gene Activation via JNK/P38 and NF-KB-Dependent Mechanisms.” *Journal of Ethnopharmacology* 127(3):662–68. doi:10.1016/j.jep.2009.12.007.
4. Drechsler, Sabine, and Jörg Andrä. 2011. “Online Monitoring of Metabolism and Morphology of Peptide-Treated Neuroblastoma Cancer Cells and Keratinocytes.” *Journal of Bioenergetics and Biomembranes* 43(3):275–85. doi:10.1007/s10863-011-9350-y.
5. Eroğlu Güneş, Canan, Fatma Seçer Çelik, Mücahit Seçme, Levent Elmas, Yavuz Dodurga, and Ercan Kurar. 2022. “Glycoside Oleandrin Downregulates Toll-like Receptor Pathway Genes and Associated MiRNAs in Human Melanoma Cells.” *Gene* 843:146805. doi:10.1016/j.gene.2022.146805.
6. Feng, Lijuan, Siqi Li, Chaoran Wang, and Jigang Yang. 2023. “Current Status and Future Perspective on Molecular Imaging and Treatment of Neuroblastoma.” *Seminars in Nuclear Medicine* 53(4):517–29. doi:10.1053/j.semnuclmed.2022.12.004.
7. Feulefack, Joseph, Aiza Khan, Francesco Forastiere, and Consolato M. Sergi. 2021. “Parental Pesticide Exposure and Childhood Brain Cancer: A Systematic Review and Meta-Analysis Confirming the IARC/WHO Monographs on Some Organophosphate Insecticides and Herbicides.” *Children* 8(12).
8. Gerges, A., and U. Canning. 2024. “Neuroblastoma and Its Target Therapies: A Medicinal Chemistry Review.” *ChemMedChem* 19(9). doi:10.1002/cmdc.202300535.
9. Gu, Min, Yuexinzi Jin, Xun Gao, Wenying Xia, Ting Xu, and Shiyang Pan. 2023. “Novel Insights into IL-37: An Anti-Inflammatory Cytokine with Emerging Roles in Anti-Cancer Process.” *Frontiers in Immunology* 14.

10. Haque, Shafiul, Arif Hussain, Hemant Joshi, Ujjawal Sharma, Bunty Sharma, Diwakar Aggarwal, Isha Rani, Seema Ramniwas, Madhu Gupta, and Hardeep Singh Tuli. 2023. “Melittin: A Possible Regulator of Cancer Proliferation in Preclinical Cell Culture and Animal Models.” *Journal of Cancer Research and Clinical Oncology* 149(19):17709–26. doi:10.1007/s00432-023-05458-8.
11. Hu, Yamei, Zigang Dong, and Kangdong Liu. 2024. “Unraveling the Complexity of STAT3 in Cancer: Molecular Understanding and Drug Discovery.” *Journal of Experimental & Clinical Cancer Research* 43(1):23. doi:10.1186/s13046-024-02949-5.
12. Huang, Jye Yu, Shu Fen Peng, Fu Shin Chueh, Po Yuan Chen, Yi Ping Huang, Wen Wen Huang, and Jing Gung Chung. 2021. “Melittin Suppresses Epithelial-Mesenchymal Transition and Metastasis in Human Gastric Cancer AGS Cells via Regulating Wnt/BMP Associated Pathway.” *Bioscience, Biotechnology and Biochemistry* 85(11). doi:10.1093/bbb/zbab153.
13. Ibrahim, Hairulislam M., Jihad Alessa, Hala Badr Khalil, Gamal A. Bekhet, and Ashraf Khalifa. 2025. “Synergistic Anti-Cancer Activity of Melittin and Erlotinib in Non-Small Cell Lung Cancer.” *International Journal of Molecular Sciences* 26(7):2903. doi:10.3390/ijms26072903.
14. Jo, Miran, Mi Hee Park, Pushpa Saranya Kollipara, Byeong Jun An, Ho Sueb Song, Sang Bae Han, Jang Heub Kim, Min Jong Song, and Jin Tae Hong. 2012. “Anti-Cancer Effect of Bee Venom Toxin and Melittin in Ovarian Cancer Cells through Induction of Death Receptors and Inhibition of JAK2/STAT3 Pathway.” *Toxicology and Applied Pharmacology* 258(1):72–81. doi:10.1016/j.taap.2011.10.009.
15. Khalil, Abdelwahab, Basem H. Elesawy, Tarek M. Ali, and Osama M. Ahmed. 2021. “Bee Venom: From Venom to Drug.” *Molecules* 26(16):4941. doi:10.3390/molecules26164941.
16. Lee, Gihyun, and Hyunsu Bae. 2016. “Anti-Inflammatory Applications of Melittin, a Major Component of Bee Venom: Detailed Mechanism of Action and Adverse Effects.” *Molecules* 21(5):616. doi:10.3390/molecules21050616.
17. Lee, Kwang-Sik, Bo-Yeon Kim, Min-Ji Park, Yijie Deng, Jin-Myung Kim, Yun-Hui Kim, Eun-Jee Heo, Hyung-Joo Yoon, Kyeong-Yong Lee, Yong-Soo Choi, and Byung-Rae Jin. 2022. “Bee Venom Induces Acute Inflammation through a H2O2-Mediated System That Utilizes Superoxide Dismutase.” *Toxins* 14(8):558. doi:10.3390/toxins14080558.
18. Li, Xinrui, Bing Yan, Jin Du, Shanshan Xu, Lu Liu, Caifei Pan, Xianhui Kang, and Shengmei Zhu. 2022. “Recent Advances in Progresses and Prospects of IL-37 in Central Nervous System Diseases.” *Brain Sciences* 12(6).
19. Li, Yan, Nuo Chen, Yaxin Guo, and Lining Zhang. 2025. “The Stress and the Alarmin-like Cytokine Interleukin-37 Mediated Extracellular and Intracellular Signal Pathways.” *Seminars in Immunology* 78:101952. doi:10.1016/j.smim.2025.101952.
20. Mansour, Ghada H., Mohammed A. El-Magd, Dalia H. Mahfouz, Ismail A. Abdelhamid, Magda F. Mohamed, Nada S. Ibrahim, Abdel Hady A. Abdel Wahab, and Emad M. Elzayat. 2021. “Bee Venom and Its Active Component Melittin Synergistically Potentiate the Anticancer Effect of Sorafenib against HepG2 Cells.” *Bioorganic Chemistry* 116. doi:10.1016/j.bioorg.2021.105329.

21. Mei, Yu, and Haiyan Liu. 2019. “IL-37: An Anti-inflammatory Cytokine with Antitumor Functions.” *Cancer Reports* 2(2). doi:10.1002/cnr2.1151.
22. Mei, Yu, Ying Zhu, Huey Yee Teo, Yonghao Liu, Yuan Song, Hwee Ying Lim, Zuhairah Binte Hanafi, Veronique Angeli, and Haiyan Liu. 2020. “The Indirect Antiangiogenic Effect of IL-37 in the Tumor Microenvironment.” *Journal of Leukocyte Biology* 107(5). doi:10.1002/JLB.3MA0220-207RR.
23. Obeidat, Maher, Ihab F. Al-khraisat, Da’san M. M. Jaradat, Bayan Y. Ghanim, Qasem M. Abdallah, Duaa Abu Arqoub, Duaa Sabbah, Ola M. Al-Sanabra, Tawfiq Arafat, and Nidal A. Qinna. 2023. “Mellitin Peptide Quantification in Seasonally Collected Crude Bee Venom and Its Anticancer Effects on Myelogenous K562 Human Leukaemia Cell Line.” *BMC Complementary Medicine and Therapies* 23(1):132. doi:10.1186/s12906-023-03897-x.
24. Palm, Noah W., Rachel K. Rosenstein, Shuang Yu, Dominik D. Schenten, Esther Florsheim, and Ruslan Medzhitov. 2013. “Bee Venom Phospholipase A2 Induces a Primary Type 2 Response That Is Dependent on the Receptor ST2 and Confers Protective Immunity.” *Immunity* 39(5):976–85. doi:10.1016/j.immuni.2013.10.006.
25. Pandey, Pratibha, Fahad Khan, Minhaj Ahmad Khan, Rajnish Kumar, and Tarun Kumar Upadhyay. 2023. “An Updated Review Summarizing the Anticancer Efficacy of Melittin from Bee Venom in Several Models of Human Cancers.” *Nutrients* 15(14):3111. doi:10.3390/nu15143111.
26. Pedro, Giovana, Felipe César da Silva Brasileiro, Rui Seabra Ferreira Jr., Aline Márcia Marques Bráz, and Renée Laufer-Amorim. 2025. “Melittin Inhibits Proliferation, Migration, and Invasion in Osteosarcoma Cell Lines Using 2D and 3D Models.” *Journal of Venomous Animals and Toxins Including Tropical Diseases*. doi:10.1590/1678-9199-JVATITD-2024-0053.
27. Pieniążek, Barbara, Katarzyna Cencelewicz, Patrycja Bździuch, Łukasz Młynarczyk, Monika Lejman, Joanna Zawitkowska, and Katarzyna Derwich. 2024. “Neuroblastoma—A Review of Combination Immunotherapy.” *International Journal of Molecular Sciences* 25(14):7730. doi:10.3390/ijms25147730.
28. Reddy, Ramakkamma Aishwarya, Magham Sai Varshini, and Raman Suresh Kumar. 2023. “Matrix Metalloproteinase-2 (MMP-2): As an Essential Factor in Cancer Progression.” *Recent Patents on Anti-Cancer Drug Discovery* 20(1). doi:10.2174/0115748928251754230922095544.
29. Shoari, Alireza, Mathew A. Coban, and Evette S. Radisky. 2025. “Therapeutic Potential of Inhibitors of Gelatinases MMP-2 and MMP-9 for the Treatment of Breast Cancer.” *The FEBS Journal*. doi:10.1111/febs.70343.
30. Singh, Nitin, Deepak Baby, JagadishPrasad Rajguru, PankajB Patil, SavitaS Thakkannavar, and VeenaBhojaraj Pujari. 2019. “Inflammation and Cancer.” *Annals of African Medicine* 18(3):121. doi:10.4103/aam.aam_56_18.
31. Sohrab, Sayed Sartaj, Riya Raj, Amka Nagar, Susan Hawthorne, Ana Cláudia Paiva-Santos, Mohammad Amjad Kamal, Mai M. El-Daly, Esam I. Azhar, and Ankur Sharma. 2023. “Chronic Inflammation’s Transformation to Cancer: A Nanotherapeutic Paradigm.” *Molecules* 28(11):4413. doi:10.3390/molecules28114413.

32. Sollberger, Gabriel, Gerhard E. Strittmatter, Martha Garstkiewicz, Jennifer Sand, and Hans-Dietmar Beer. 2014. “Caspase-1: The Inflammasome and Beyond.” *Innate Immunity* 20(2):115–25. doi:10.1177/1753425913484374.
33. Sun, Hongyi, Jie Ding, Yujia Jiang, Danying Zhang, Jin Yu, Shuai Sun, Jing Zhou, and Chaoqin Yu. 2025. “Melittin Inhibits Ovarian Cancer Cell Growth by Downregulating MMP9 Expression via the JAK2-STAT3 Signaling Pathway.” *Current Medicinal Chemistry* 32. doi:10.2174/0109298673355946250403071132.
34. Tomolonis, Julie A., Xin Xu, Kshiti H. Dholakia, Chunchao Zhang, Linjie Guo, Amy N. Courtney, Siyue Wang, Julien Balzeau, Gabriel A. Barragán, Gengwen Tian, Erica J. Di Pierro, and Leonid S. Metelitsa. 2023. “Interaction between Tumor Cell TNFR2 and Monocyte Membrane-Bound TNF-α Triggers Tumorigenic Inflammation in Neuroblastoma.” *Journal for ImmunoTherapy of Cancer* 11(3):e005478. doi:10.1136/jitc-2022-005478.
35. Voronov, Elena, Dror S. Shouval, Yakov Krelin, Emanuela Cagnano, Daniel Benharroch, Yoichiro Iwakura, Charles A. Dinarello, and Ron N. Apte. 2003. “IL-1 Is Required for Tumor Invasiveness and Angiogenesis.” *Proceedings of the National Academy of Sciences of the United States of America* 100(5). doi:10.1073/pnas.0437939100.
36. Wang, Anqi, Yuan Zheng, Wanxin Zhu, Liuxin Yang, Yang Yang, and Jinliang Peng. 2022. “Melittin-Based Nano-Delivery Systems for Cancer Therapy.” *Biomolecules* 12(1):118. doi:10.3390/biom12010118.
37. Wang, Kangli, Lingchen Tao, Meifei Zhu, Xinyu Yu, Yuanyuan Lu, Bin Yuan, and Fuliang Hu. 2024. “Melittin Inhibits Colorectal Cancer Growth and Metastasis by Ac-Tivating the Mitochondrial Apoptotic Pathway and Suppressing Epithelial–Mesenchymal Transition and Angiogenesis.” *International Journal of Molecular Sciences* 25(21):11686. doi:10.3390/ijms252111686.
38. Wei, Rongfei, Xiao Han, Mengyuan Li, Yuan Ji, Lianfeng Zhang, Maria Ioanna Christodoulou, Najwa Jameel Hameed Aga, Caiyan Zhang, Ran Gao, Jiangning Liu, Jinrong Fu, Guoping Lu, Xiaojun Xiao, Xiaoyu Liu, Ping Chang Yang, Iain B. McInnes, Ying Sun, Peisong Gao, Chuan Qin, Shau Ku Huang, Yufeng Zhou, and Damo Xu. 2023. “The Nuclear Cytokine IL-37a Controls Lethal Cytokine Storms Primarily via IL-1R8-Independent Transcriptional Upregulation of PPARγ.” *Cellular and Molecular Immunology* 20(12). doi:10.1038/s41423-023-01091-0.
39. Wu, Ruixin, Ning Li, Weiling Huang, Yifang Yang, Rongrong Zang, Haiyan Song, Jianrong Shi, Shiguo Zhu, and Qing Liu. 2025. “Melittin Suppresses Ovarian Cancer Growth by Regulating SREBP1-Mediated Lipid Metabolism.” *Phytomedicine* 137:156367. doi:10.1016/j.phymed.2025.156367.
40. Yan, Rucheng, Weiwei Dai, Yuanshen Mao, Guopeng Yu, Wenfeng Li, Minfeng Shu, and Bin Xu. 2023. “Melittin Inhibits Tumor Cell Migration and Enhances Cisplatin Sensitivity by Suppressing IL-17 Signaling Pathway Gene LCN2 in Castration-resistant Prostate Cancer.” *The Prostate* 83(15):1430–45. doi:10.1002/pros.24605.
41. Yao, Xiang, Junlong Kang, Yufei Li, Haoran Zhang, Zhibin Yang, and E. Chen. 2024. “Melittin Protects against Neural Cell Damage in Rats Following Ischemic Stroke.” *Neuropeptides* 107:102462.

doi:10.1016/j.npep.2024.102462.

42. Zamani, Mozhdeh, Farzaneh Bozorg-Ghalati, and Pooneh Mokarram. 2024. “Melittin as an Activator of the Autophagy and Unfolded Protein Response Pathways in Colorectal HCT116 Cell Line.” *Iranian Biomedical Journal* 28(1):46–52. doi:10.61186/ibj.3993.
43. Zhao, Qiwu, Haoran Feng, Zheyu Yang, Juyong Liang, Zhijian Jin, Lingxie Chen, Ling Zhan, Ming Xuan, Jiqi Yan, Jie Kuang, Xi Cheng, Ren Zhao, and Weihua Qiu. 2022. “The Central Role of a Two-way Positive Feedback Pathway in Molecular Targeted Therapies-mediated Pyroptosis in Anaplastic Thyroid Cancer.” *Clinical and Translational Medicine* 12(2). doi:10.1002/ctm2.727.

Tables

Table 1. Primer Sequences for Target Genes.

Gen	Accession Number	Primer	Sequences (5'→3')
β-aktin	AY582799.1	F	CCACGAAACTACCTTCAACTCC
		R	GTGATCTCCTTCTGCATCCTGT
MMP2	NM_001302510.2	F	TGATGGTGTCTGCTGGAAAG
		R	CTACAGGACAGAGGGACTAGAG
IL-37a	NM_014439.4	F	AAAAAGATGAACCCCAGTGC
		R	TTTAGAGACCCCCAGGAGAA
IL-1R8 (SIGIRR)	NM_001135054.2	F	ACCTGCTCCATCCAGAACAT
		R	TTCCCGTCGTTTATCTCCAC
IL-18R1	NM_003855.5	F	CACTGATAGAGAAAAGCCGAAGA
		R	ATTGGGGCAAGAATGTGAAG
MMP9	NM_004994.3	F	CGGACCAAGGATACAGTTTG
		R	CGCCCAGAGAAGAAGAAAAG
NF-κB	NM_001382627.1	F	GCAATCATCCACCTTCATTCT
		R	ATCCTCCACCACATCTTCCT
STAT3	NM_001384993.1	F	AAGTCAGGTTGCTGGTCAAA
		R	TGCCGTTGTTGGATTCTTC
MyD88	NM_001172567.2	F	GGCAACTGGAACAGACAAAC
		R	TAATCATCAGAGACAACCACCA
Caspase-1	NM_001257118.3	F	AAGGGAGGAGAGAAAAGCCA
		R	TCGGAATAACGGAGTCAATCAA
Smad3	NM_001407016.1	F	GCTACCTGAGTGAAGATGGAGA
		R	AGTTGGGAGACTGGACAAAAA

Table 2: Gene Symbol Mapping and Functional Roles in KEGG Pathways

Gene Name in Study	HGNC Symbol	Role in KEGG Pathways
IL-37a	IL-37	Anti-inflammatory cytokine; regulation of innate immune responses; involved in cytokine–cytokine receptor interaction and immune tolerance pathways.
IL-1R8 (SIGIRR)	SIGIRR	Negative regulator of Toll-like receptor (TLR) and IL-1 signaling pathways; modulates inflammatory signaling and NF-κB pathway suppression.
IL-18R1	IL18R1	Part of Toll-like receptor signaling, cytokine–cytokine receptor interaction, Th1 differentiation, and NF-κB activation pathways.
NF-κB	NFKB1	Master transcription factor in inflammatory response, TNF signaling, TLR signaling, apoptosis regulation, and cell survival pathways.
STAT3	STAT3	Key mediator of JAK-STAT signaling, PI3K-Akt signaling, cell survival, inflammation, and oncogenesis.
MyD88	MYD88	Central adaptor protein in Toll-like receptor (TLR) and IL-1 receptor signaling, leading to activation of NF-κB and MAPK pathways.
Caspase-1	CASP1	Regulator of inflammasome activation, pyroptosis, and IL-1β/IL-18 maturation; involved in innate immunity and programmed cell death.
Smad3	SMAD3	Signal transducer in the TGF-β signaling pathway, regulating apoptosis, inflammation, fibrosis, and cell cycle progression.
MMP-2	MMP2	Matrix degradation enzyme involved in ECM remodeling, cell migration, angiogenesis, and metastasis pathways.
MMP-9	MMP9	Matrix metalloproteinase involved in extracellular matrix degradation, invasion, inflammation, and metastasis-related signaling pathways.

Table 3. Summary of the highest-ranking molecular docking results of melittin with STAT3 and IL-1R8

Target Protein	PDB ID	Docking Score	Confidence Score	Ligand RMSD (Å)
IL-1R8 (SIGIRR)	6D65	**-296.74**	**0.9495**	46.97
STAT3	6NJS	**-200.27**	0.7321	37.17

Table 4. Key *in silico* ADMET properties of melittin predicted using ADMETlab 3.0.

Property Category	Parameter	Predicted Value	Unit/Classification	Interpretation & Relevance
Physicochemical	Molecular Weight (MW)	2844.75	Da	Very high; typical for peptides, suggests poor oral bioavailability.
	Hydrogen Bond Donors (nHD)	50	-	Far exceeds optimal range (0-7); major challenge for oral absorption and permeability.
	Hydrogen Bond Acceptors (nHA)	70	-	Far exceeds optimal range (0-12); major challenge for oral absorption and permeability.
	Topological Polar Surface Area (TPSA)	1152.34	Å²	Extremely high; far exceeds optimal range (0-140 Å²) indicating very low membrane permeability.
Medicinal Chemistry	Synthetic Accessibility (SAscore)	9.0	-	Very difficult to synthesize chemically (SAscore ≥ 6).
Absorption	Caco-2 Permeability	-7.851	Log unit	Very low permeability (Optimal: > -5.15).
	Human Intestinal Absorption (HIA+)	1.0	Probability	High probability of poor intestinal absorption.
	P-glycoprotein Inhibitor	1.0	Probability	High probability of being a P-gp inhibitor; risk of drug-drug interactions.
Distribution	Fraction Unbound (Fu)	133.67	%	Very high plasma protein binding; may limit tissue availability.
	Blood-Brain Barrier (BBB+)	0.0	Probability	Very low probability of crossing the BBB; favorable for reducing potential neurotoxicity.
Toxicity	hERG Blockers	0.031	Probability	Very low risk of cardiotoxicity via hERG channel blockade.
	Drug Induced Liver Injury (DILI)	0.0	Probability	Very low risk of drug-induced liver injury.

	Drug-induced Nephrotoxicity	1.0	Probability	High risk of kidney damage; a known concern for melittin.
	Drug-induced Neurotoxicity	0.984	Probability	High risk of neurotoxicity; a known concern for melittin.
	AMES Mutagenicity	0.003	Probability	Very low risk of mutagenicity.

Figures

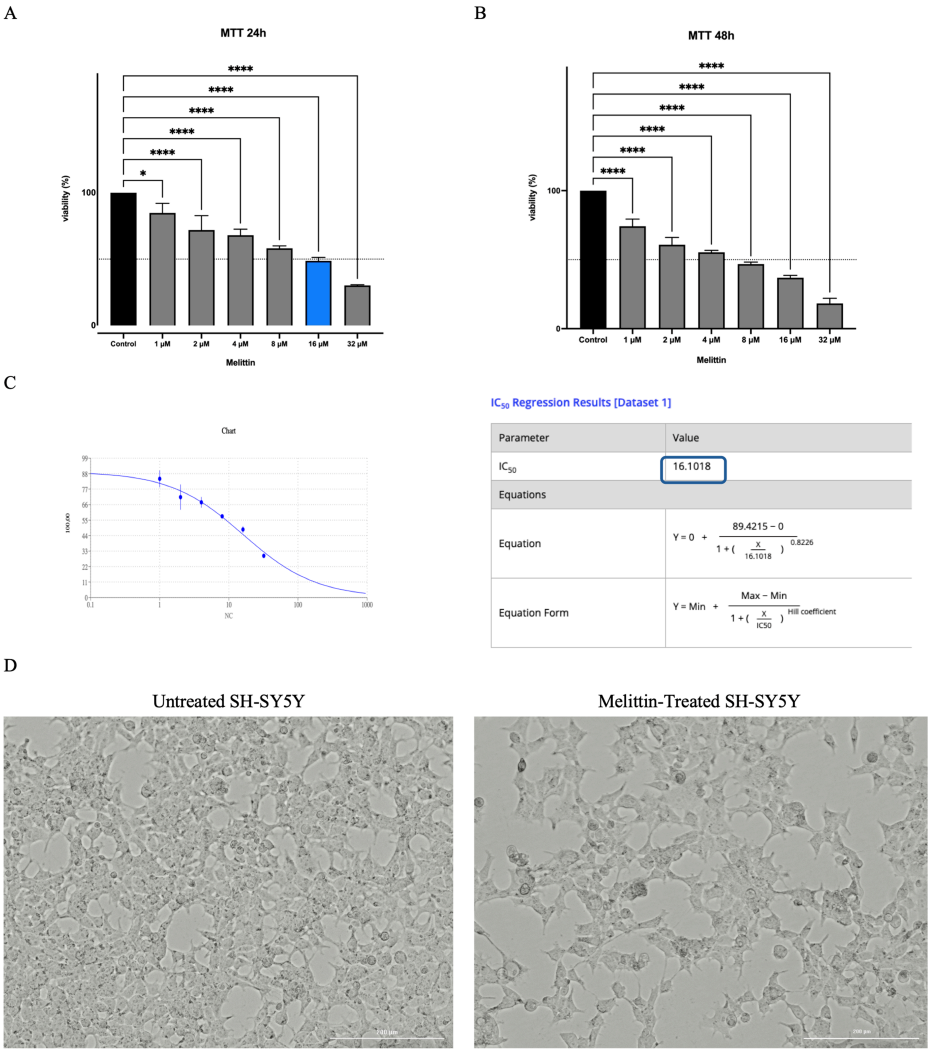


Figure 1

Melittin reduces the viability of SH-SY5Y neuroblastoma cells in a dose- and time-dependent manner.

MTT assay showing SH-SY5Y cell viability following melittin treatment for (A) 24 h and (B) 48 h. Cell viability decreased below 50% at concentrations ≥16 µM after 24 h and >4 µM after 48 h. (C) IC_{50} value of melittin (16 µM at 24 h) calculated using the AAT Bioquest IC_{50} calculator. (D) Representative brightfield

microscopy images of SH-SY5Y cells treated with melittin at the IC_{50} concentration (16 µM, 24 h). Data are presented as mean ± SD (n = 3) and were analyzed using GraphPad Prism 10. *p < 0.05, **p < 0.01, ***p < 0.001, ****p < 0.0001 versus control.

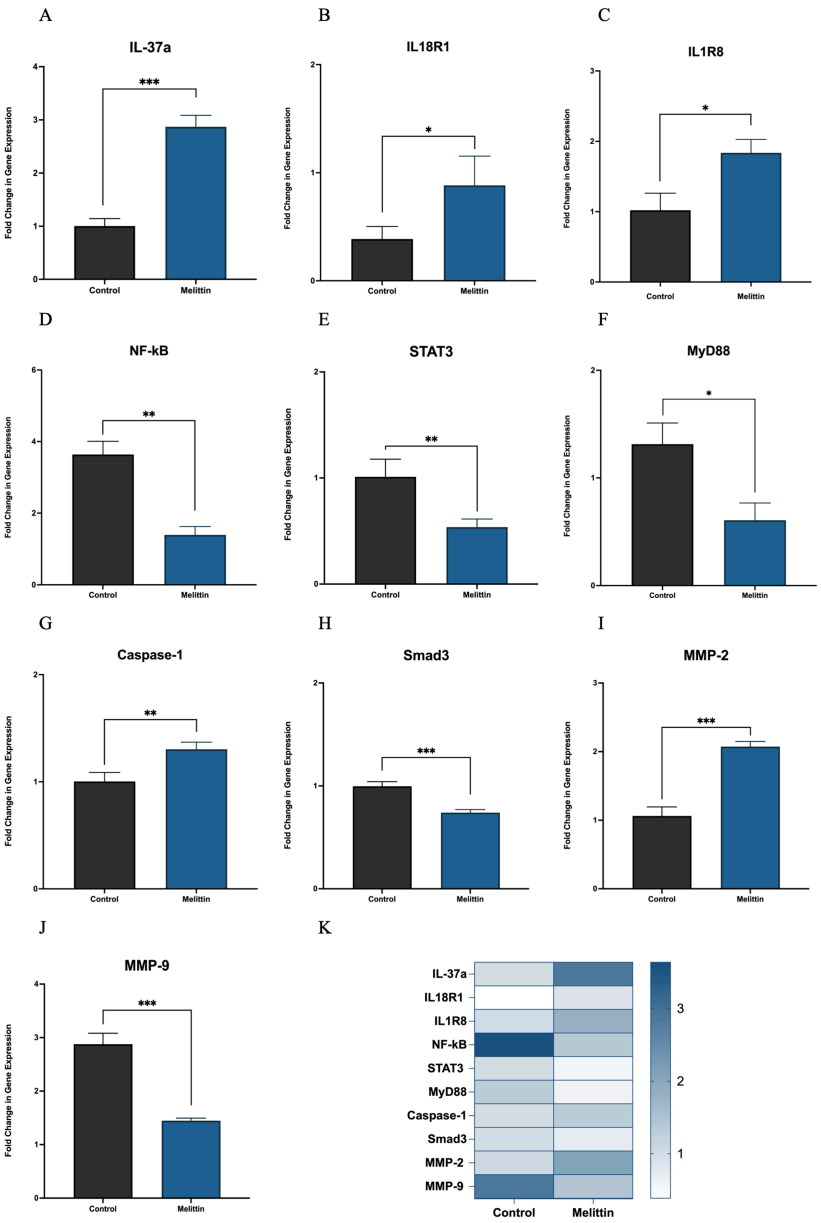


Figure 2

Melittin induces an IL-37a-centered anti-inflammatory transcriptional response in SH-SY5Y cells. Gene expression changes in SH-SY5Y cells treated with melittin (16 μM, 24 h) compared with untreated control cells. qRT–PCR analyses were performed for (A) IL-37a, (B) IL-18R1, (C) IL-1R8 (SIGIRR), (D) NF-κB, (E)STAT3, (F) MyD88, (G) Caspase-1, (H) Smad3, (I) MMP-2, and (J) MMP-9. (K) Heatmap illustrating global transcriptional profiles and hierarchical clustering patterns between treatment groups. Data are presented as mean ± SD (n = 3) and were analyzed using GraphPad Prism 10. *p < 0.05, **p < 0.01, ***p < 0.001 versus control.

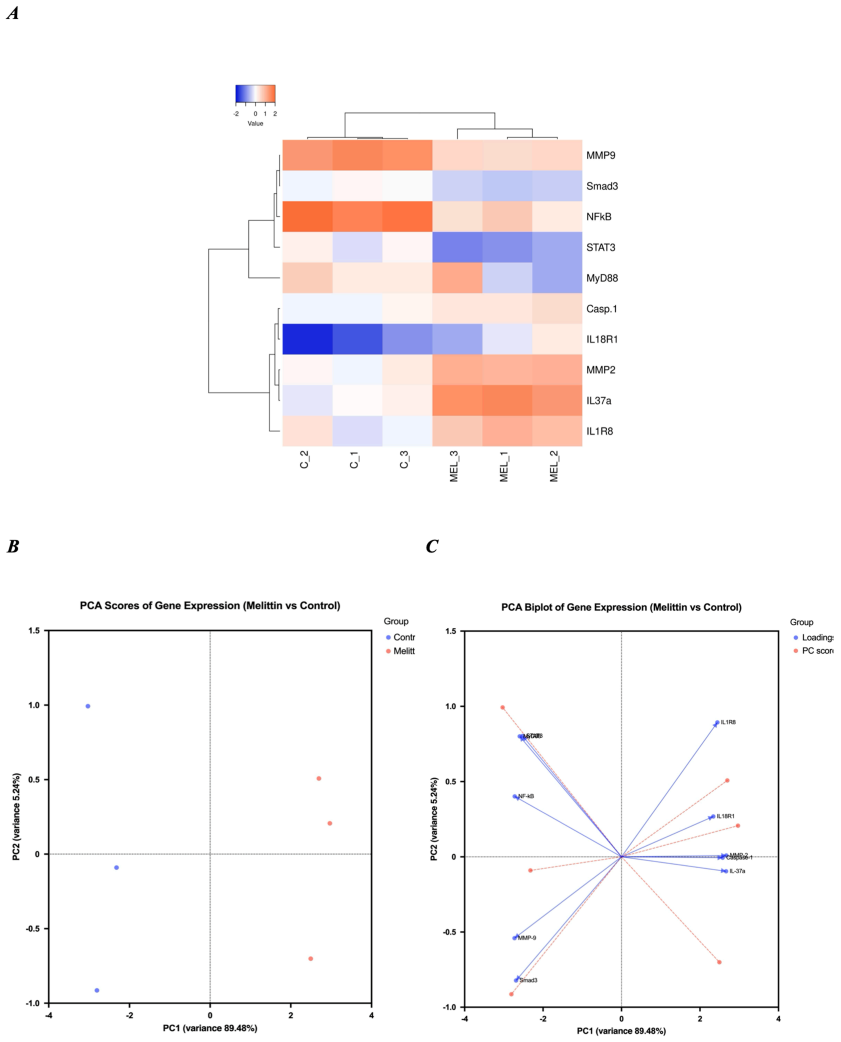


Figure 3

Multivariate analysis of gene expression patterns in melittin-treated SH-SY5Y cells.
(A) Hierarchical clustering heatmap of genes associated with inflammation, immune regulation, and extracellular matrix remodeling. The analysis was performed using three biological replicates for each group (control and melittin-treated; $n = 3$). Differential expression was evaluated using thresholds of $|\log_2 FC| \geq 1$ and adjusted $p < 0.05$.
(B) PCA score plot showing complete separation of melittin-treated replicates from control replicates along PC1, which accounts for 89.48% of the total variance, while PC2 explains 5.24%.
(C) PCA biplot illustrating the direction and magnitude of gene contributions to the principal components. IL-37a, IL-1R8, IL-18R1, Caspase-1, and MMP-2 load positively along PC1, whereas NF-κB, STAT3, MyD88, Smad3, and MMP-9 load negatively along PC1.

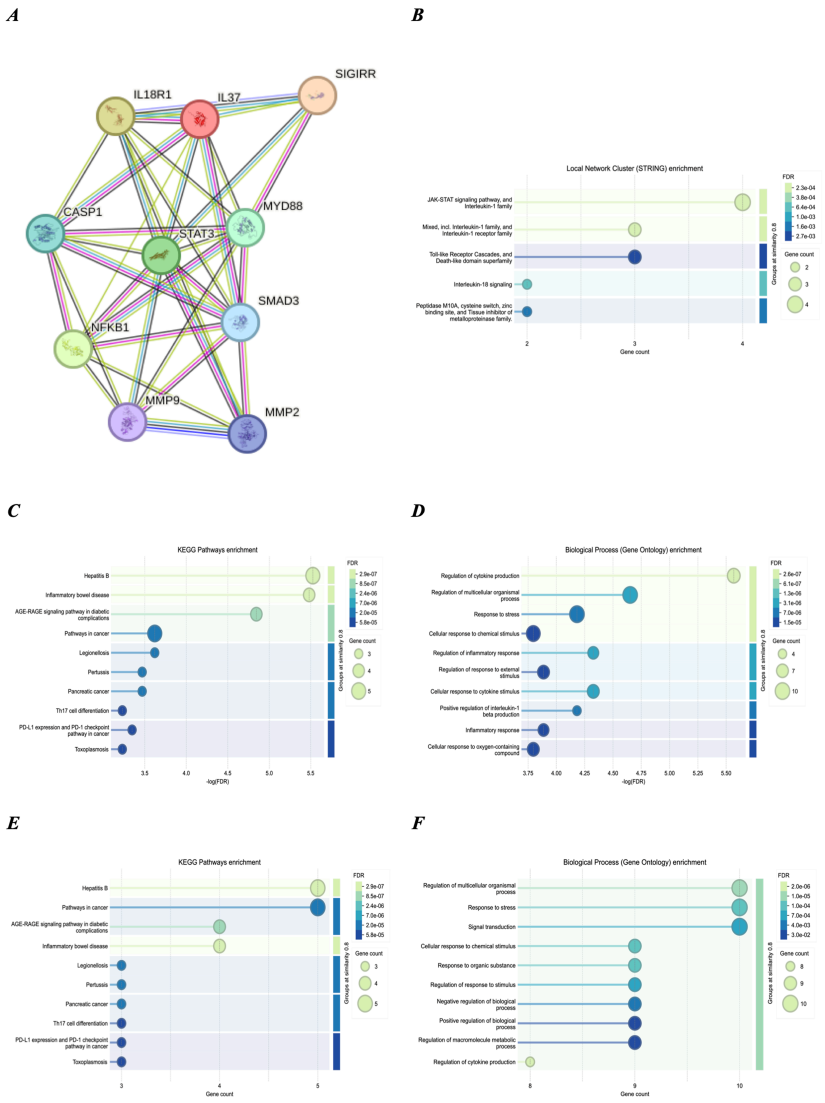


Figure 4

STRING network architecture and GO/KEGG enrichment analysis of melittin-responsive genes in SH-SY5Y cells.

(A) STRING-based protein–protein interaction (PPI) network illustrating functional relationships among genes regulated by melittin.

(B) STRING local network cluster enrichment analysis showing pathway-level functional clustering of the associated gene groups.
(C) KEGG pathway enrichment analysis ranked by −log(FDR) values and (E) KEGG analysis based on gene contribution counts, highlighting significantly enriched pathways.
(D) Gene Ontology (GO) Biological Process enrichment ranked by −log(FDR) values and (F) GO enrichment based on gene contribution counts, demonstrating enrichment of biological processes related to inflammatory responses, stress-associated signaling pathways, cytokine production, and extracellular matrix remodeling.

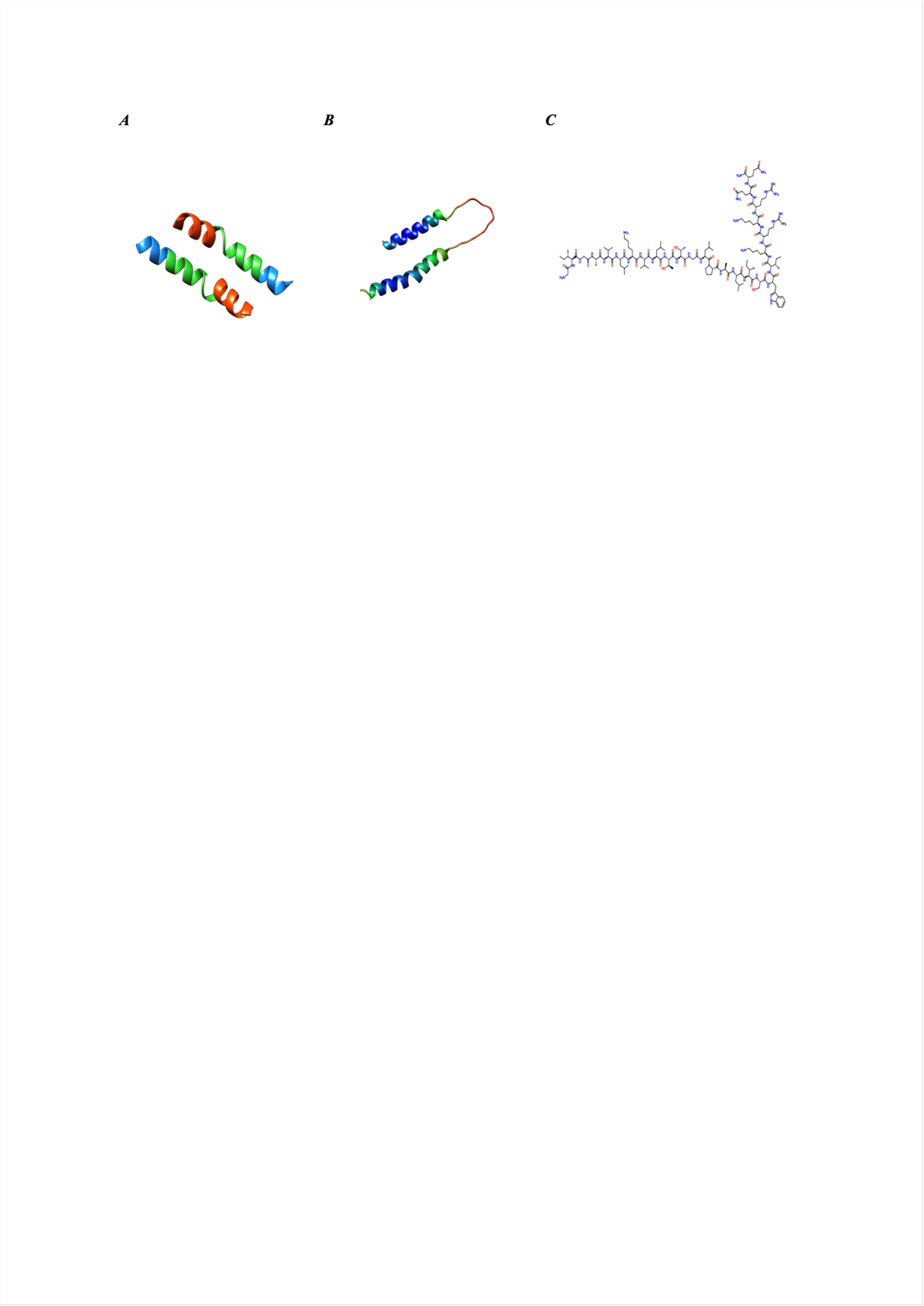


Figure 5

Structural comparison of experimental and predicted melittin models.
(A) Ribbon representation of the experimentally determined crystal structure of melittin (PDB ID: 2MLT) visualized using UCSF Chimera. Residues are colored with a continuous gradient from the N-terminus (blue) to the C-terminus (red) to highlight the α-helical architecture.
(B) AlphaFold-predicted structure of melittin (UniProt ID: P01501). The model is colored according to per-

residue pLDDT confidence scores, with blue indicating high-confidence regions and yellow-to-red tones representing lower-confidence, flexible regions.
(C) Two-dimensional chemical structure of melittin illustrating its amino acid composition and peptide backbone connectivity.



Figure 6

Molecular docking models of melittin in complex with IL-1R8 and STAT3.
(A) Overall view of the melittin–IL-1R8 complex, with melittin shown in ribbon representation (yellow). The structure corresponds to the highest-scoring docking model with a docking score of −296.74.
(B) Overall view of the melittin–STAT3 complex, with melittin shown in ribbon representation (yellow). This model corresponds to a docking score of −200.27.

Supplementary Files

This is a list of supplementary files associated with this preprint. Click to download.

- graphicalabstract.jpeg